Enhanced Raman scattering with one monolayer of silver

J. Miragliotta and T. E. Furtak
Department of Physics, Colorado School of Mines, Golden, Colorado 80401
(Received 2 October 1986)

Adatoms, clusters, and complexes have been associated with the active sites that enable the short-range mechanism of surface-enhanced Raman scattering (SERS). To clarify this relationship we have studied the interaction between pyridine and a monolayer (ML) of Ag on a Pt substrate as a function of applied potential and solution composition. Our electromagnetic calculations show only small optical fields exist at the 1-ML Ag—Pt substrate surface which are incapable of supporting the electromagnetic enhancement of SERS. This confirms our earlier report that enhancement for this system arises from an electronic resonant Raman process in the surface complex. The growth of the Ag ML was performed in a thin-layer solution-exchange electrochemical cell. The cell allowed removal of the Ag^+ solution and introduction of a pyridine and Cl^- solution while maintaining a constant applied potential. Results reported here show that no SERS exists for pyridine adsorbed on the pre-prepared Ag ML. Electrochemical oxidation and reduction of the ML in the presence of pyridine and Cl^- is necessary before a signal is observed. This process creates Cl^--stabilized, electron-deficient sites onto which pyridine is bound. These Ag^+ sites on the Pt substrate are analogous to the Ag_4^+ pyramidal clusters which have been discovered as SERS-active sites on bulk Ag substrates.

I. INTRODUCTION

Since the first report of surface-enhanced Raman scattering (SERS) in 1974,[1] numerous studies have been performed to determine the underlying mechanisms of this surface phenomena.[2] Although these studies have shown the overall enhancement can be divided into two distinct groups, controversy still exists as to the relative importance of these individual mechanisms to the total observed enhancement. The first group, referred to as electromagnetic or optical enhancement, arise primarily on rough (50—300 Å) noble-metal surfaces such as Ag, Cu, and Au.[3–6] The surface-roughness features can support optical resonances (surface plasmon-polaritons) which enhance the incident local field as well improve coupling between the Raman-shifted scattered light and the observed far field radiation. The second mechanism, which is not clearly understood, involves a resonant Raman process in the metal—adsorbed-molecule surface complex.[7–11] This mechanism is referred to as a chemical or short-range enhancement process and tends to be sensitive to the surface site ("active site") of the adsorbed molecule.

In earlier studies it was not always possible to eliminate the electromagnetic enhancing properties of a surface when investigating the short-range mechanism of SERS.[12–15] Most experiments were performed on noble-metal surfaces which contributed an optical component to the observed enhancement. Mechanistic studies should be performed on surfaces of materials such as Pt or Ni where the optical resonances would be damped by other electronic processes, e.g., interband transitions.[16–18] This would enable independent study of the short-range mechanism of SERS without competing enhancement from electromagnetic mechanisms.

This report is an extension of an earlier paper which introduced our approach of investigating the short-range component of SERS using a Pt substrate in the electrochemical environment.[19] We are interested in duplicating, as closely as possible, the surface chemistry that exists in active Ag substrates. To that end, our program has involved careful deposition and characterization of Ag monolayers on a Pt substrate using electrochemical methods. The enhancement that arises at the electrode-electrolyte interface is not general to other interfacial systems. For instance, enhanced scattering from a single metal monolayer on a metallic substrate has only been observed in the electrochemical environment. This may be due to the intrinsic difference in the nature of the liquid-solid and gas-solid interfaces, e.g., the large electrostatic forces that exist at the former due to the arrangement of charge in the double layer. In our work reported upon previously it was only possible to monitor the pyridine—silver-monolayer interaction at potentials positive of the reversible Nernst potential (0.365 V) since bulk Ag deposition occurred negative of this value. In this report, we have investigated the pyridine—silver-monolayer—Pt-substrate system as a function of applied potential and solution composition, *without* the complication of Ag bulk deposition.

The growth of the Ag monolayer (ML) on the Pt surface is known to occur uniformly, without Ag particle formation.[20] Uniformity is a critical requirement for this system, since Ag particles give rise to electromagnetic enhancement at the metal surface. As will be shown in Sec. II, the uniform Ag ML alone can *not* sufficiently increase the poor electromagnetic enhancing properties of the underlying Pt substrate, i.e., the surface remains electromagnetically inactive. Any enhancement that may arise at this surface must be considered short-range in na-

ture.

To perform the above SERS investigation of the pyridine—silver-monolayer interaction it was necessary to construct a new electrochemical cell. The major requirement of the cell was that it allow separate, well-controlled deposition processes at the sample surface. For example, it was essential that the initial Ag ML deposition on the Pt substrate occur in a pyridine-free solution so as to avoid co-deposition of these two species. To accommodate the requirement, a convenient solution-exchange flushing system was designed which provided easy removal of one cell solution for another while maintaining a constant applied potential. Figure 1 shows an exploded view of the new cell. We refer to this apparatus as a thin-layer solution-exchange electrochemical cell. As will be evident from a detailed discussion in Secs. III and IV, this cell allows the investigation of surfaces that could not be created in a conventional bulk-solution electrochemical cell.

We shall emphasize a number of points throughout this report. First, one can exclude electromagnetic enhancement of SERS for a molecule adsorbed on a pre-prepared Ag ML since only small optical fields exist at this surface. Second, an observable SERS signal is possible only after the pre-prepared Ag ML is oxidized and then reduced in a pyridine and Cl^- solution. This result is similar to that observed in previous works, including ourselves, in which SERS was detected after co-deposition of Ag^+ and pyridine on a Pt substrate.[16,17,19] Finally, only with the new solution exchange cell could the SERS from the pyridine—silver-monolayer formation be investigated as a function of applied potential.

II. THEORY

For a Ag ML deposited on a perfectly smooth Pt surface, it is not possible for an incident electromagnetic field to excite surface plasmon-polaritons on the metal surface. This is due to the wave-vector mismatch between the incident field and the surface plasmon at all frequencies (except $\omega=0$). On such a surface an additional momentum source such as a surface grating is needed to facilitate the excitation. Coupling on a rough metal surface can occur since the roughness features destroy the translational invariance of the smooth surface, eliminating the requirement of momentum conservation parallel to the interface.

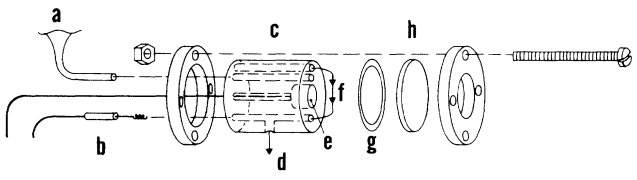

FIG. 1. Exploded view of the thin-layer electrochemical sample chamber. The assembly is held together with four screws, only one of which is shown. (a) Glass fixture through which electrical contact with the reference electrode (not shown) is made. (b) Pt wire counter electrode. (c) Main body of the chamber, Teflon. (d) Output for solution flow. (e) Sample. (f) Schematic representation of the direction of solution flow. (g) Teflon gasket-spacer. (h) Quartz window.

This roughness is in general random in dimension, but assumed much smaller than the wavelength of the incident light. A more complete discussion of surface plasmons and roughness is presented in Ref. 21 for the interested reader. The Pt surface used in our experiment has roughness features due to the mechanical polishing techniques used to prepare the sample. While it is not possible to excite a surface plasmon on the bare Pt substrate in the optical frequency region, the possibility arises that a Ag ML adsorbed on this surface may allow a resonance to occur. We will now demonstrate that this is of no concern.

Previous theories dealing with the electromagnetic characteristics of rough metal surfaces usually limit the roughness geometries to simple structures such as hemispheroids and spheroids.[3,4,22] This allows tractable solutions for the enhancing properties of these particles. For our purposes, we have used the model employed by Murray in which the substrate and surrounding metal overlayer are considered a confocal pair of prolate spheroids.[23–25] We refer to the inner spheroid of the pair as that volume containing only Pt. The term "outer spheroid" refers to the entire spheroidal system. The spheroid is defined by an effective dielectric permittivity[26]

$$\epsilon_{\text{eff}}=\frac{\epsilon_2[(\epsilon_1-\epsilon_2)(vA_2-A_1-v)-\epsilon_1]}{(\epsilon_1-\epsilon_2)(vA_2-A_1)-\epsilon_2}\ , \tag{1}$$

where v is the volume ratio of the inner and outer spheroid, ϵ_1 and ϵ_2 are the complex dielectric functions of Pt and Ag, respectively, and A_1 and A_2 are the inner and outer depolarization factors. The values of ϵ_1 and ϵ_2 as a function of wavelength were taken from the literature.[27,28] Expressions for v, A_1, and A_2 are given in Ref. 23.

In our simple model, we assume the outer spheroid is small compared to the wavelength of the incident field, $\lambda_0=514.5$ nm (Rayleigh approximation). This is a reasonable approximation since we have restricted the size of the particle to <300 Å. The problem of calculating the local fields reduces to one of electrostatics rather than electrodynamics.[29] Throughout the calculations, we directed the incident field along the semimajor axis of the outer spheroid, defined as the z direction. All field and enhancement values were determined for a molecule located at the tip of the outer spheroid. For the thin Ag overlayer we have modified the imaginary part of the dielectric function by including a term which accounts for electron scattering from the boundaries of the overlayer.[30] This term increases the effective electron scattering rate in the overlayer, leading to a reduction in the optical fields outside the spheroid.

We discovered a printing error in Murray's article which under certain conditions gives incorrect values for the electromagnetic enhancement of SERS. The discrepancy arises in the expression for the local field at the tip of the outer spheroid (Ref. 23, Eq. 5). The correct expression is[31]

$$E_{\text{tip}}=E_0\left[1+\frac{(\epsilon_{\text{eff}}-\epsilon_3)(1-A_2)/\epsilon_3}{1+A_2(\epsilon_{\text{eff}}-\epsilon_3)/\epsilon_3}\right]\hat{\mathbf{z}}\ , \tag{2}$$

where E_0 is the incident field and ϵ_3 is the dielectric function of the medium surrounding the ellipsoid. The $1/\epsilon_3$

factor in the numerator of the second term in Eq. (2) is missing in Murray's expression.

The electromagnetic enhancement for SERS will be proportional to the total dipole moment of the molecule-spheroid system. Thus, we define this enhancement as

$$G = |\mu_t|^2 / |\mu_0|^2 , \tag{3a}$$

where

$$|\mu_t|^2 = [\alpha E_{\text{tip}}(\omega_0)]^2 [\alpha E_{\text{tip}}(\omega_s)]^2 , \tag{3b}$$

$$|\mu_0|^2 = |\alpha E_0|^4 , \tag{3c}$$

μ_t, μ_0, and α are the total dipole moment of the molecule-spheroid system, dipole moment in the absence of enhancement, and the molecular polarizability of the molecule, respectively. We have used Eq. (2) for the field at the tip of the spheroid. The electromagnetic enhancement is proportional to the product of the field intensity at the incident frequency, ω_0, and that at the scattered frequency, ω_s. This expression does *not* include any contribution that may arise from the molecule's dipole image in the spheroid.

Figure 2 shows a plot of G versus the incident photon energy for a molecule adsorbed at the tip of a Ag spheroid. The dimensions of the particle were chosen for optimum electromagnetic enhancement at the incident wavelength of 514.5 nm (2.41 eV). The outer semimajor and minor axes are 150 and 65 Å, respectively. The dimensions of the outer spheroid were fixed at these values throughout all calculations.

To determine the effects of an inner spheroid of Pt on the SERS enhancement G, we removed a volume of Ag from the center of the spheroid and replaced it with an equal amount of Pt. Figures 3 and 4 show the results of the procedure. As is evident from the figures, G shows a marked decrease and broadening in its resonance position as the volume of the inner Pt spheroid is increased. We note that the ratio of the inner semimajor and semiminor axes are identical to that of the outer axes, assuring a uniform Ag overlayer on the inner Pt spheroid as the Pt volume was increased. The dashed curve in Fig. 4 is for a spheroid containing an average Ag overlayer thickness of 6.3 Å. The average thickness was determined by taking the difference between the arithmetic mean of the outer and inner spheroid axes.

Note that only a small electromagnetic SERS enhancement is possible for a molecule at the tip of the Ag-coated

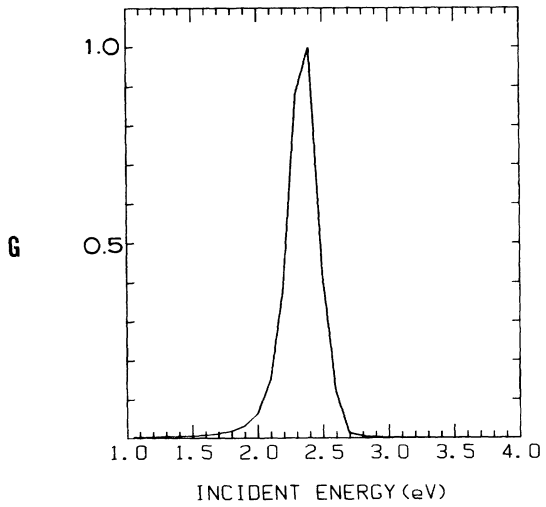

FIG. 2. Normalized electromagnetic enhancement of SERS, G, vs incident photon energy for a Ag spheroid with semimajor to semiminor axis ratio (a/b) of 165 Å/65 Å.

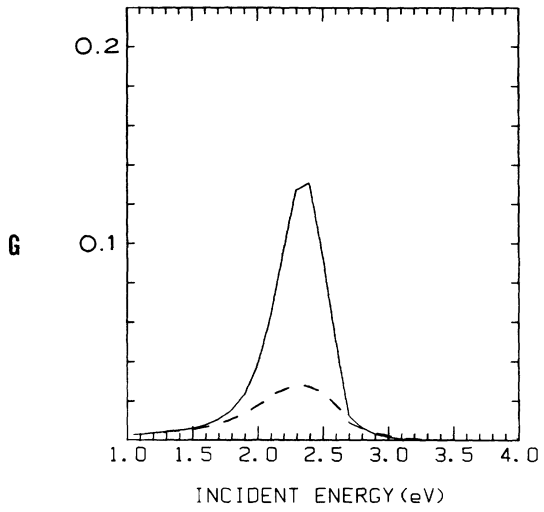

FIG. 3. Electromagnetic enhancement of SERS, G, vs incident photon energy for various Ag/Pt spheroids. Scale is $\frac{1}{5}$ of Fig. 2. Solid curve has a Pt core with $a/b = 75$ Å/32.5 Å. Dashed curve has a Pt core with $a/b = 100$ Å/43.3 Å.

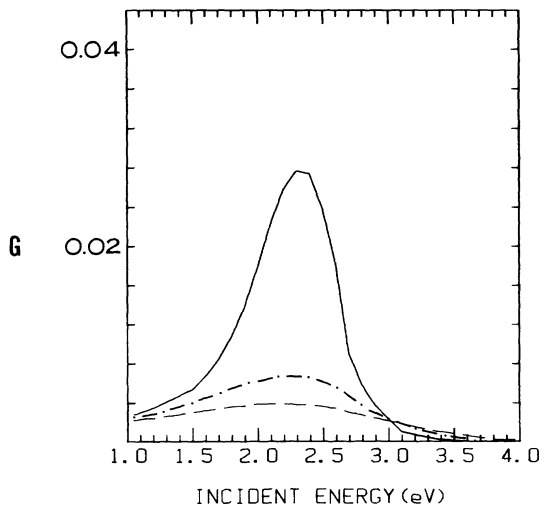

FIG. 4. Electromagnetic enhancement of SERS, G, vs incident photon energy for various Ag/Pt spheroids. Scale is $\frac{1}{25}$ of Fig. 2. Solid curve has a Pt core with $a/b = 100$ Å/43.3 Å. Dot-dashed curve has a Pt core with $a/b = 125$ Å/54.1 Å. The dashed curve has a Pt core with $a/b = 140$ Å/60.6 Å. The Ag overlayer for this final curve has an electron mean free path of 20 Å.

Pt spheroid. The damping of the optical fields outside these particles are due to the shortened electron mean free path in the Ag ML and interaction of the plasmon fields with the inner Pt spheroid. The latter influence leads to low-energy interband transitions in this core providing additional damping for electromagnetic resonances.

Since a uniform Ag ML will occupy <3 Å average overlayer thickness, Fig. 4 (dashed curve) can be considered an upper limit on the electromagnetic enhancement ability of the Ag ML—Pt substrate surface. Therefore, any SERS that may arise at this surface will *not* be electromagnetic in nature. This justifies our assumption that our experiments deal primarily with the short-range mechanism of SERS.

III. PROCEDURE

The body of the thin-layer solution-exchange cell consisted of a polycrystalline Pt sample (99.99%, 0.25-in.-diameter rod) mounted in a 1.0-in-diameter Teflon rod so as to be concentric and planar with the rod surface. The thin-layer solution chamber was constructed by placing a Teflon gasket (0.002 in) between the planar surface of the body and a S1-UV quartz window. A pressure seal between the gasket and window created the thin layer above the sample and also eliminated the problem of leaks during the exchange of the sample chamber. The solution exchange was performed using a versatile inlet-outlet system which consisted of two small-bore holes leading from the back of the body to the front planar surface. The Pt counterelectrode was placed in the outlet chamber so as to avoid sample contamination during solution exchange. For similar reasons, a third chamber was designed to isolate the saturated calomel reference electrode (SCE) from the thin-layer chamber while keeping electrical contact with the Pt sample. A small-bore hole leading from the back of the body to Pt sample provided a means of electrical contact to the electrode. These specifications are represented in Fig. 1.

Prior to each experiment the sample was mechanically polished, ending with 0.05-μm alumina. It was then ultrasonically cleaned for 5 min in triply distilled water and then soaked in a solution of 25% nitric acid, 25% sulfuric acid, and triply distilled water. The sample was then soaked in triply distilled water until the thin-layer cell was assembled. The quartz window was cleaned with Alconox detergent, soaked in the above acid mixture, and then rinsed in triply distilled water. All solutions were composed of reagent-grade chemicals and triply distilled water. Before introduction into the thin-layer cell, the solutions were purged with zero-grade nitrogen for 30 min. The applied potential was controlled with a Pine potentiostat and all electrochemical records were collected with a Houston x-y recorder. Triangular potential scans were generated by the potentiostat, and current through the sample was plotted as a function of applied potential. All electrochemical data were recorded with a potential scan rate of 1 V/min.

Raman spectra were obtained with the double-monochromater—photon-counting system described in our previous work. The monochromator was set to two regions of interest, 80—320 cm^{-1} and 950—1070 cm^{-1}, at 120 cm^{-1}/min. Both ranges had data point resolutions of 2.1 cm^{-1}. The number of repeat scans per spectra was dependent upon signal strength. The incident excitation was p polarized at 514.5 nm and 200 mW in a line focus on the sample. The angle of incidence was 45°.

All Raman data were collected at constant applied potentials, with the collection lens of the monochromator focused on and perpendicular to the sample surface. Scattered light within a solid angle of 40 msr about this perpendicular line was admitted to the monochromator.

IV. RESULTS

A. Electrochemical records

Prior to each experiment the Pt sample was electrochemically monitored for surface purity in $0.1M$ $Na_2SO_4 + 0.1M$ H_2SO_4. The applied potential was scanned between -0.27 and $+0.9$ V (SCE) until reproducible hydrogen adsorption and desorption peaks were obtained in the current versus potential records, as shown in Fig. 5. Adsorption peaks at -0.1 and -0.23 V (negative-current peaks) correspond to the strongly and weakly bound species of atomic hydrogen, respectively.[32] The actual surface area of the Pt sample was determined by measuring the charge delivered during the hydrogen adsorption process and comparing this to the standard amount of 210 $\mu C/cm^2$.[33] We found a surface-roughness factor of 1.4 for the sample.

The procedure of growing a stable and uniform Ag ML is illustrated in Fig. 6. The cell solution for this electrochemical record was $(1.5\times10^{-3})M$ $AgNO_3 + 0.01M$ $Na_2SO_4 + 0.01M$ H_2SO_4. The applied potential was

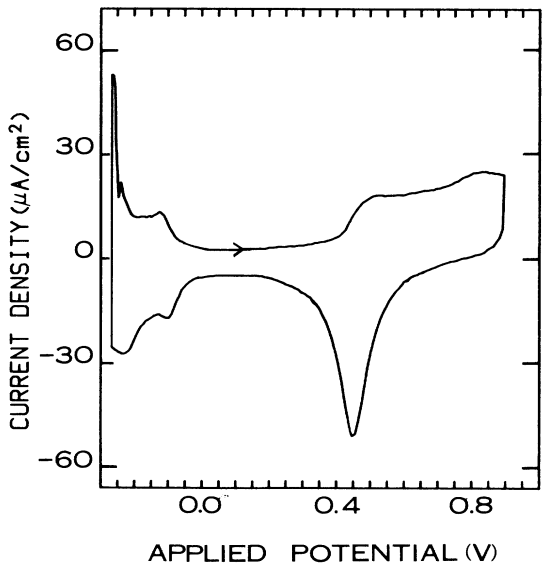

FIG. 5. Sample current versus applied potential for Pt in $0.01M$ $H_2SO_4 + 0.1M$ Na_2SO_4. The scan rate was 1 V/min. Applied potential (V) with respect to the saturated calomel electrode (SCE).

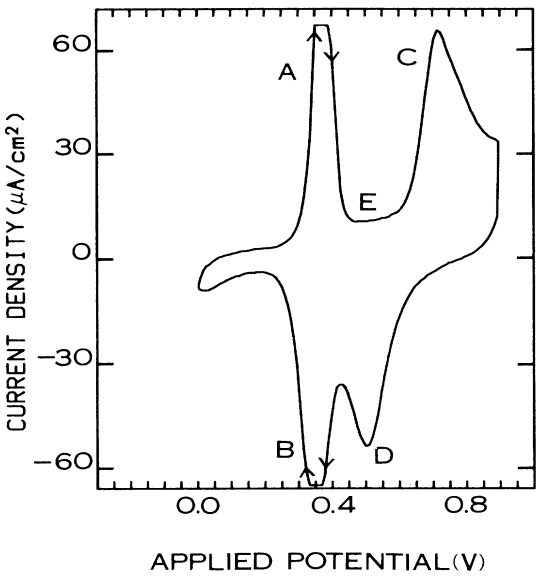

FIG. 6. Sample current versus applied potential for Pt in $0.1M$ $H_2SO_4 + 0.1M$ $Na_2SO_4 + (1.5\times10^{-3})M$ $AgNO_3$. The scan rate was 1 V/min. Applied potential (V) with respect to the saturated calomel electrode (SCE).

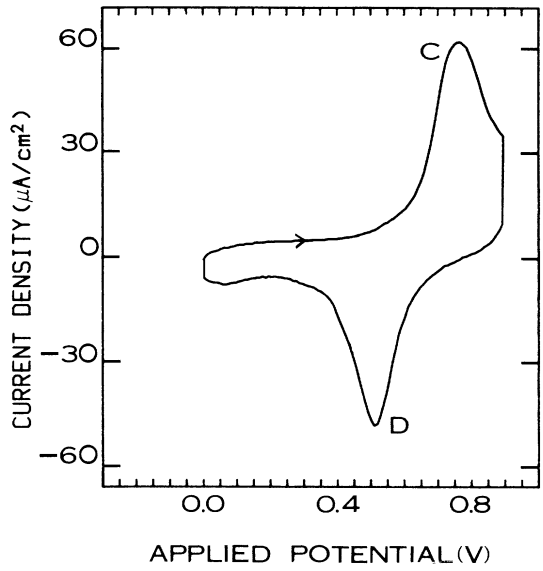

FIG. 7. Sample current vs applied potential for an Ag ML—Pt surface in $0.01M$ $H_2SO_4 + 0.1M$ Na_2SO_4. The scan rate was 1 V/min. Applied potential (V) with respect to the saturated calomel electrode (SCE).

scanned between 0.0 and 0.9 V until reproducible Ag multilayer and monolayer oxidation peaks (herein referred to as "stripping" peaks) were obtained. These two, well-separated processes (0.38 V) are denoted in Fig. 6 as A and C, respectively. After achieving a reproducible record the potential was held at E (+ 0.55 V), which is between the Ag multilayer stripping potential and the Ag ML stripping potential. The Ag^+ solution was then flushed from the cell with $0.01M H_2SO_4 + 0.1M$ Na_2SO_2 leaving *only* 1 ML of Ag on the Pt surface and eliminating the possibility of further Ag deposition. The applied potential was again scanned between 0.0 and + 0.9 V to ensure that *only* Ag ML adsorption and stripping occurred at the Pt surface. The record of this scan is shown in Fig. 7, with the adsorption and stripping processes denoted C and D, respectively. In our previous work, it was not possible to investigate or prepare an Ag ML without co-deposition with pyridine. However, as discussed above, the thin-layer cell allowed preparation of the Ag ML with little difficulty.

After the pre-prepared Ag ML was grown on the sample, a $0.025M$ pyridine + $0.1M$ KCl solution was introduced into the cell at an applied potential of 0.0 V. Figure 8 shows the electrochemical process of oxidizing and reducing the Ag ML in the pyridine and Cl^- solution. The applied potential was scanned from 0.0 to + 0.8 V then back to −0.1 V. We emphasize that the Ag coverage on the surface is no greater than 1 ML during this scan. In previously reported studies Ag bulk deposition occurred for potential negative of the reversible Nerant potential (0.365 V) making it impossible to study the pyridine—silver-monolayer interaction at these potentials.

We believe peaks A and B correspond to Cl^- adsorption and desorption on the Ag ML, while peaks C and D represent oxidation of the residual Ag on the Pt surface. We shall refer to the electrochemical process in Fig. 8 as the "activation" of the Ag ML.

B. Raman spectra

The surface Raman scattering from pyridine adsorbed on the pre-prepared Ag ML are shown in Figs. 9 and 10(a). The cell solution was $0.025M$ pyridine + $0.1M$

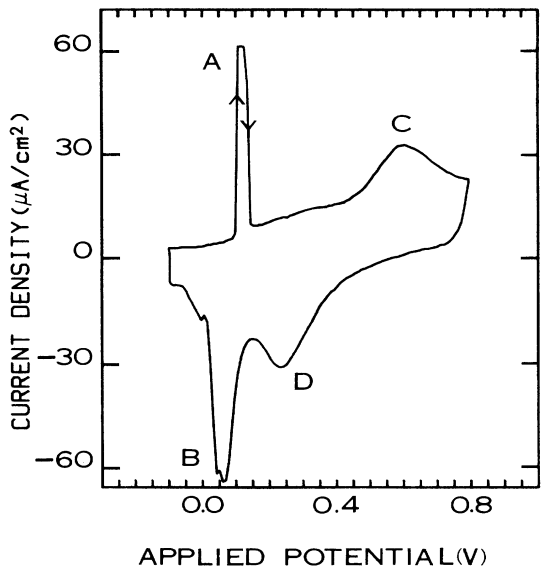

FIG. 8. Sample current versus applied potential for a Ag ML—Pt surface in $0.1M$ KCl + $0.025M$ pyridine. The scan rate was 1 V/min. Applied potential (V) with respect to the saturated calomel electrode (SCE).

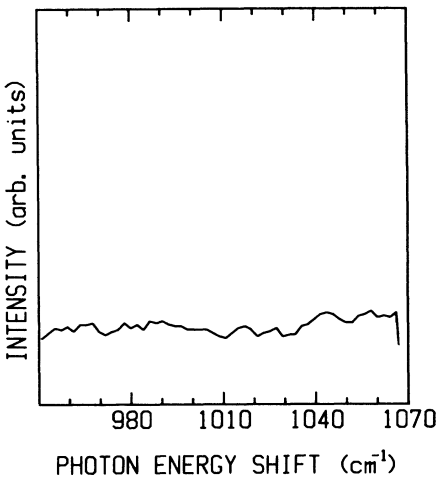

FIG. 9 Surface Raman spectrum for the Ag ML—Pt in 0.1M KCl + 0.025M pyridine prior to electrochemical activation (Fig. 8). The applied potential was −0.1 V. Identical spectra were obtained at −0.2 and −0.3 V (not shown).

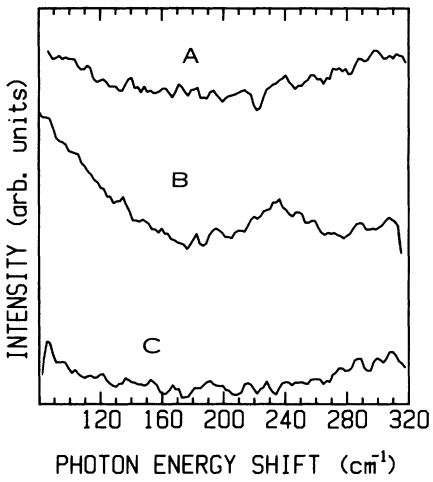

FIG. 10. Raman spectra obtained from Ag ML—Pt surface. (a) The applied potential was −0.1 V and no electrochemical activation (Fig. 8) was performed. Cell solution was 0.1M KCl + 0.025M pyridine. (b) The applied potential was −0.1 V. Recorded after electrochemical activation in 0.025M pyridine + 0.1M KCl. (c) The applied potential was −0.1 V. Recorded after electrochemical activation in 0.1M KCl followed by introduction of 0.025M pyridine.

KCl and no activation of the Ag ML had been performed. As shown in Fig. 9 no detectable signal was observed over the photon energy shift of 950 to 1070 cm^{-1} at the applied potentials of −0.1, −0.2, and −0.3 V. A similar result was found in the 80 to 320 cm^{-1} spectrum [Fig. 10(a)] which was recorded at −0.1 V. Note the absence of normal Raman scattering from pyridine in bulk solution. The vibrational modes of pyridine in solution are usually observed at 1008 and 1037 cm^{-1}. However, the incident radiation interacts with only a small volume of solution in the thin-layer chamber, thus contributing only a negligible term to the spectra. No SO_4^{-2} mode at 978 cm^{-1} is present since the counterion in solution is Cl^-. Our previous investigation required SO_4^{-2} as the counterion to avoid AgCl precipitation in the cell solution.

The spectrum in Fig. 10(b) was recorded at −0.1 V after two activation cycles had been performed in 0.025M pyridine + 0.1M KCl. The spectrum shows a small broad peak centered at 235 cm^{-1} whose magnitude remained constant with time. Figure 10(c) was recorded after the Ag ML was activated in a 0.1M KCl solution (no pyridine), followed by the introduction of pyridine at −0.1 V. Again, we were unable to detect any signal under these conditions.

The data in Fig. 11(a) show a large peak at 1020 cm^{-1} with smaller peaks at 1008 and 1037 cm^{-1}. The spectrum was recorded at −0.1 V immediately after two activation cycles of the Ag ML in 0.025M pyridine + 0.1M KCl. The magnitude of the 1020 cm^{-1} mode remained constant with time at this applied potential. Figures 11(b) and 11(c) show the effect of applying a potential more negative than −0.1 V. The magnitude of the 1020 cm^{-1} mode decayed with time at −0.2 V and became undetectable at −0.3 V. The behavior of this 1020 cm^{-1} mode is similar to that of the 1018 cm^{-1} mode on multilayer Ag in our last article.[19] At potentials more negative than that of the bulk deposition peak the 1018 cm^{-1} mode also disappeared. This suggests the negative potential induced the destruction of resonant surface complexes which were responsible for the short-range mechanism of SERS. It is likely the 1020 and 1018 cm^{-1} modes arise from very similar surface complexes.

To reestablish a SERS signal after destruction of the signal at −0.3 V, activation of the Ag ML was performed in the pyridine and Cl^- solution. After the activation, the applied potential was stepped to 0.0 V, and the spectrum shown in Fig. 12(a) was recorded. The magnitude of the 1020 cm^{-1} mode remained constant with time, similar to the spectrum recorded at −0.1 V [Fig. 11(a)]. The spectrum in Fig. 12(b) was taken at + 0.2 V which is on the

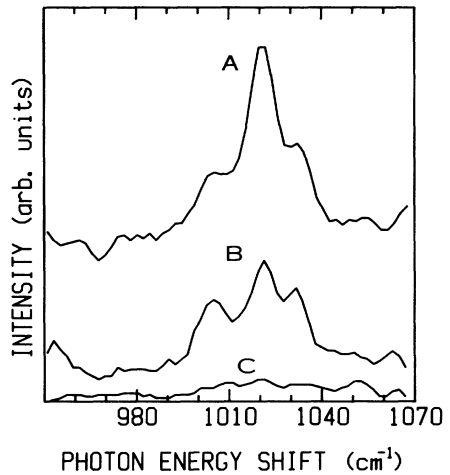

FIG. 11. Raman spectra obtained from Ag ML—Pt surface after electrochemical activation (Fig. 8). (a) The applied potential was −0.1 V. (b) The applied potential was −0.2 V. (c) The applied potential was −0.3 V.

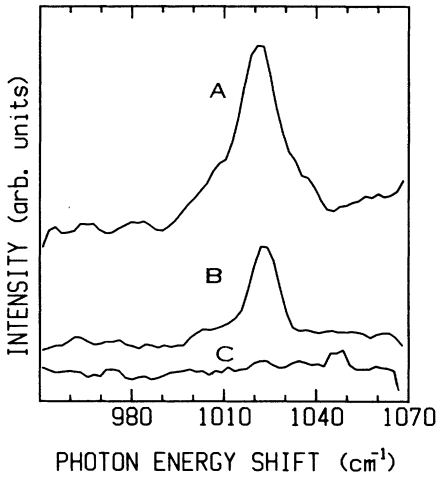

FIG. 12. Raman spectra obtained from the Ag ML—Pt surface after electrochemical activation (Fig. 8). (a) The applied potential was 0.0 V. (b) The applied potential was + 0.2 V. (c) The applied potential was + 1.0 V.

positive side of the AgCl formation peak (peak *A*, Fig. 8). There is a 3 cm^{-1} shift in the 1020 cm^{-1} mode compared to the position of the mode at −0.1 V. The shift was accomplished by a decrease in SERS intensity; however, the signal remained constant with time.

The final spectrum [Fig. 12(c)] was recorded at + 1.0 V, beyond the stripping peak of the residual Ag on Pt (peak *C*, Fig. 8). No Ag remained on the surface at this potential. Under these conditions no detectable SERS was observed.

V. DISCUSSION

A. Electrochemical results

For a Pt electrode in equilibrium with an Ag^+ solution, it is known that deposition occurs in two separate, well-defined regions of applied potential. Deposition first proceeds with the growth of a uniform Ag ML at potentials on the positive side of the reversible Nernst potential (underpotential deposition). Separation of these two processes is due to Ag interacting more strongly with the underlying Pt than with a corresponding surface of Ag. Although no theoretical treatment for underpotential deposition presently exists, investigations of various monolayer-substrate couples in the electrochemical environment has led to an empirical expression relating the potential difference of the bulk and monolayer stripping peaks to the difference in the work functions of the two metals. The physical model for underpotential deposition was introduced by Kolb, Przasayski, and Gerischer[34] and agrees reasonably well with a number of metal couples including Ag/Pt. Results for vapor-deposited Ag in ultrahigh vacuum (UHV) on single-crystal Pt surfaces show the deposition process also occurs in two distinct steps pointing to the similarity between the Ag-Pt interaction in the two experimental systems.[35]

Experimentally, it is known that up to 1.54 ML of Ag is deposited on Pt *before* bulk deposition can occur.[36] The Ag ML formation has been shown to proceed uniformly, free of Ag clusters on the surface. During multilayer deposition these structures can form on the surface, providing sites for optical field enhancement. However, all spectra in this work were recorded under conditions of Ag ML coverage, eliminating any possibility of electromagnetic enhancement as shown in Sec. II.

The electrochemical record in Fig. 3 shows the charge-transfer processes that occur on Pt as a function of applied potential in an Ag^+ cell solution. Peaks *A* and *B* demonstrate Ag bulk stripping and deposition, respectively. The position of these peaks (+ 0.37 V) agrees with the calculated Nernst potential in the Ag^+ cell solution. Both bulk processes occur in the same potential region, indicating a high degree of reversibility during the surface reaction. The potential separation of peaks *A* and *C* (0.38 V) agrees with previous electrochemical studies of Ag on Pt.[36–38] We note that the potential difference gives a measure of relative bonding strength of the Ag-Pt and Ag-Ag interactions.

Peaks *C* and *D* in Fig. 3 show Ag ML stripping and deposition, respectively, on the Pt surface. Unlike the corresponding bulk Ag processes, the Ag ML stripping and deposition occur simultaneously with other charge-transfer surface reactions. Peak *C* represents both Ag ML stripping and Pt oxide formation, leading to an observed charge transfer of 2.1 ML of material. Conversely, peak *D* corresponds to Ag ML formation and oxygen desorption on the Pt surface. Due to the complex nature of this reaction, there is a degree of irreversibility for these respective processes (*C* and *D*).

After removal of the Ag^+ cell solution, stripping and deposition of Ag on Pt in $0.1M$ $Na_2SO_4 + 0.01M$ H_2SO_4 was recorded in Fig. 4. The procedure of eliminating Ag^+ solution ensured only 1 ML of Ag deposited on the surface (*C* and *D*). Despite a slight positive shift in peak *C* (relative to the same peak in Fig. 3) the process of ML adsorption and desorption remained unchanged in the Ag^+-free solution. We attribute this independence to the thin layer of solution above the sample surface which eliminated the mass transport of Ag^+ to and from the interfacial region at the applied potential scan rate of 1 V/min.[39] This also suggests that the equilibrium between the surface and Ag^+ in solution for the monolayer reaction occurs only in the metal solution interface region with little or no influence of the Ag^+ concentration in the bulk solution. This is contrary to the Ag bulk deposition process, which is strongly dependent on the Ag^+ cell solution concentration.

To determine the Ag coverage on the Pt surface, the applied potential was scanned into the hydrogen adsorption region (0.0→−0.27 V). Previous studies of Ag on Pt show that a complete Ag ML (210 $\mu C/cm^2$) inhibits hydrogen adsorption by approximately 85% with respect to a bare Pt substrate.[40] Our result (not shown here) found the Ag/Pt surface inhibited this adsorption process by 70%, indicating an Ag coverage of approximately 80%. This is a uniform coverage, since Fig. 4 shows only a Ag-Pt interaction at the Pt surface.

The electrochemical record in Fig. 5 shows the oxida-

tion and reduction of the Ag ML in a pyridine and Cl^- solution. This represents the first time Ag^+ and pyridine co-deposit on the Pt surface in this experiment. All previous SERS investigations of the pyridine-silver interaction on Pt were performed under these conditions.[16,17,20] Peaks $A \rightarrow D$ denote charge-transfer processes that occur upon scanning the applied potential between -0.1 and $+0.8$ V. To our knowledge, such a result has not previously appeared in the literature. We believe the process in peak A corresponds to the oxidation of the Ag ML into an insoluble layer of AgCl. Peak B is the subsequent reduction of the metal halide layer on the negative scan of the applied potential. These two peaks are analogous to the oxidation and reduction of a bulk Ag substrate in a pyridine and Cl^- solution.[13]

Peaks C and D are more difficult to interpret. We believe the formation of the AgCl layer (peak A) is only partial, leaving bare Ag sites on the Pt surface. Peak C represents the stripping of these sites from the Pt substrate as the applied potential is scanned positive. Subsequently, peak D shows the redeposition of the Ag on the negative potential scan. This hypothesis is supported by a number of results. First, the charge transfer observed in peaks C and D represents approximately 50% of the total Ag coverage. Second, SERS from the surface is observed between peaks A and C, but is undetectable beyond the positive side of peak C. We also note that the positions of C and D are identical to our previous results of Ag^+ and pyridine co-deposition and stripping on Pt. To completely clarify these charge-transfer reactions, further investigation is needed.

B. Raman spectra

The results presented in Figs. 9 and 10(a) were recorded under conditions of pyridine (Pyr) adsorption on the preprepared electrode surface. No activation of the Ag ML had been performed (Fig. 5) making it impossible for the Cl^- stabilized Ag^+-Pyr complex to exist at the Pt surface. Under these surface conditions it is not unusual that no SERS signal is observed. Previous experiments on bulk Ag substrates have shown the importance of a strong stabilizing agent (such as Cl^-) on the relative strength of the SERS signal.[9,41] The absence of Cl^- at the Ag/Pt allows the Ag^+-Pyr complex to dissociate (or inhibit the formation) at the surface. Also, as was discussed in Sec. II, electromagnetic enhancement is not possible at the Ag ML—Pt substrate since only small optical fields exist at this surface. A similar result occurs when pyridine is adsorbed on a bulk Ag substrate prior to oxidation and reduction of the Ag surface in a pyridine and Cl^- solution. The SERS signals at 1008 and 1037 cm^{-1} are considerably weaker than the same vibrational modes after activation of the surface, suggesting the major contribution to the former SERS signals arise from the electromagnetic enhancing properties of the underlying Ag surface.

Figure 10(b) was recorded at -0.1 V after the Ag ML was activated in a $0.025M$ pyridine $+0.1M$ KCl solution. The spectrum reveals a broad vibrational mode at 235 cm^{-1} which we attribute to a Ag-Cl surface vibration. The activation allows co-deposition of Ag^+ and pyridine on the Pt surface, which prior to this step had not occurred at the surface. Some ambiguity had existed in the literature as to whether this low-energy mode was associated with a Ag-N (pyridine) surface vibration. However, numerous investigations of this vibrational mode in both our laboratory and elsewhere have shown it is indeed a Ag-Cl mode.[42,43] Figure 10(c) was recorded after the Ag ML was activated in $0.1M$ KCl followed by the introduction of $0.025M$ pyridine at -0.1 V. The absence of SERS dramatizes the importance of performing the activation in *both* pyridine and Cl^- in forming the Ag^+-Pyr Cl^- stabilized complex. Again, this result is analogous to SERS investigations of bulk Ag substrates in pyridine and Cl^- solutions.

Figure 11(a) was recorded at -0.1 V immediately after the spectrum in Fig. 10(b). The observed mode at 1020 cm^{-1} is consistent with the symmetric ring-breathing vibration of pyridine chemisorbed to an electron-deficient Ag site (Lewis acid site). This result is similar to our previous report of an Ag^+-Pyr complex formed on the Pt substrate in a SO_4^{-2} solution.[20] In that investigation, the mode was observed at 1018 cm^{-1}, suggesting a minor role of the counterion on the observed Raman shift. It is likely that the Cl^- ion influences this mode more than SO_4^{-2} since the latter only weakly adsorbs on the electrode surface.

Some confusion exists as to whether this mode (1020 cm^{-1}) is due to adsorbed pyridine or its protonated form, pyridinium, at the metal surface. Careful pH studies have shown that the observed SERS on Ag substrates in low pH solutions arise primarily from adsorbed pyridinium.[44,45] The observed modes have been assigned to the ring-breathing (1009—1011 cm^{-1}) and the ring-stretching (1026 cm^{-1}) mode of pyridinium. Conversely, in higher pH solutions where the concentration ratio of pyridine to pyridinium. [Pyr]/[PyrH^+], is greater than 1, the dominant surface species is pyridine. In our studies, the solution pH was 5.4. The relationship between species concentration and solution pH is given by

$$pK_a = \log_{10}[\mathrm{PyrH}^+]/[\mathrm{Pyr}][\mathrm{H}^+] + p\mathrm{H} .$$

Pyridine has a pK_a (dissociation constant) $= 5.25$. Therefore, pyridine has a higher solution concentration than its protonated form. We can be assured that our signal arises from pyridine and *not* pyridinium. We note that a ring-breathing pyridinium mode was also present when the species was adsorbed on the electrode surface. No such mode is observed in our spectra, further supporting our position that our signal arises from Lewis-acid-bonded pyridine.

These Raman results, together with the preceding electromagnetic calculations in Sec. II, are evidence for an electronically resonant surface complex at the Pt substrate. There is little doubt that the resonance involves the Ag^+-Pyr structure since no appreciable SERS has been observed from pyridine adsorbed on a bare Pt substrate. However, the form of the Ag^+ surface site (cluster, adatom) remains unknown. Due to the strong Ag-Pt interaction, it is likely that the active sites are individual Ag^+ adatoms since the above interaction leads to a uni-

form Ag coverage on the Pt substrate.

Figures 11(b) and 11(c) were recorded at potentials more negative than that of -0.1 V. The resulting decrease of the 1020 cm^{-1} mode is an indication of two simultaneous processes occurring at the surface. The first is the neutralization of the Ag^+-Pyr surface complex to Ag-Pyr. The Ag site can no longer be considered electron deficient, thus the 1020 cm^{-1} mode decreases. Second, the negative bias desorbs the remaining Cl^- from the surface allowing the Ag^+-Pyr complex to dissociate. It is not possible to regain the SERS signal by returning to -0.1 V, further supporting our position that SERS arises from specific "active sites" on the Pt substrate. The above destruction procedure has also been shown to occur on bulk Ag substrates. It is conceivable that both the Ag substrate and Ag ML active sites are similar in form. Recently, evidence has been shown that active sites on the Ag surface resemble Ag_4^+ clusters, which are characterized by low-frequency vibrational modes.[46] Their detection on the Ag substrate is very difficult at best, and was not possible on a poor electromagnetic-field-enhancing substrate like Pt. In our previous article, the application of a negative bias also destroyed the Ag^+-Pyr mode at 1018 cm^{-1} on multilayer Ag. However, there was an observable SERS signal at 1008 and 1037 cm^{-1} suggesting that pyridine remains weakly adsorbed at the Ag multilayer surface.

Figure 12(a) was recorded at 0.0 V after first reestablishing the SERS signal by activating the Ag ML as in Fig. 5. We reemphasize the importance of forming the Ag^+-Pyr complex during this activation. The signal of this applied potential is very similar to the spectrum in Fig. 11(a) (-0.1 V). The stability of the signal is representative of the stability of the absorbed surface complex at 0.0 V. Figure 12(b) was recorded at an applied potential of $+0.2$ V, which is more positive than that of the partial AgCl layer formation potential. Note the 3-cm^{-1} shift of the ring-breathing mode from 1020$\rightarrow$1023 cm^{-1}. This is further evidence of the role of the counterion on the observed Raman shift. A Cl^- dependent shift of the ring-breathing mode of pyridine was observed in an earlier Raman study of pyridine adsorbed on a η-alumina powdered sample.[47] In that investigation, the observed pyridine mode at 1019 cm^{-1} shifted to 1022 cm^{-1} upon chlorination of the η alumina. The authors presumed that the adsorbed Cl^- strongly coordinated the surface species of pyridine, which then gave rise to the observed 1022 cm^{-1} mode. The remark that previous observations of this Raman "electron-deficient" vibrational mode were done in systems that contained Cl^- or ClO_4.[1,16] It is possible that there is considerable influence of Cl^- on the electron density of the $A_1\pi$ orbitals of pyridine. An increase in the orbital electron density would lead to an increase in the observed frequency of the symmetric ring-breathing mode of pyridine. We did not observe any counterion related shift of the Raman signal in our previous article; however, as mentioned earlier, SO_4^{-2} is less likely to be specifically adsorbed at the surface than is Cl^-.

The final spectrum, Fig. 12(c), was recorded at potentials more positive than that of the stripping peak of the residual Ag on Pt. Such a result would be expected only if the residual sites were indeed responsible for the observed SERS at $+0.2$ V [Fig. 12(b)]. The absence of SERS at the potential is identical to the results obtained in our previous work under the same surface conditions, i.e., no Ag on the Pt substrate. Although the potential dependence of the SERS signal at 1020 cm^{-1} is similar to the behavior of the 1008 cm^{-1} mode of pyridine bound to an active site on a bulk Ag substrate, there is an intrinsic difference between these two surfaces. The electron-deficient nature of the Ag ML on Pt is evident by the observation of the SERS signal at 1020 cm^{-1}, yet one does not generally observe this vibrational mode on a Ag substrate except after extreme pretreatment of this surface. To understand why such a difference in surface charge density should arise for these two systems, an examination of the interaction of the Ag adatom with these two respective substrates (Ag and Pt) is required. Adsorption of a Ag adatom on a bulk Ag surface is likely to shift and broaden the $5s$ electronic level of the adatom such that the level coincides with the Fermi energy of the underlying Ag metal. This process, however, leaves the Ag adatom in a neutral state. Upon replacing the underlying Ag with Pt, an electron transfer from the Ag adatom to the Pt occurs due to the difference in work functions of these respective metals. This charge transfer leaves a partial positive charge on the Ag adatom, which is consistent with the observation of SERS at 1020 cm^{-1}. It should be noted that this hypothesis is also presented for other noble-metal-overlayer—Pt systems. In previous UHV experiments of Ag, Au, and Cu overlayers on Pt surfaces, a marked decrease in the work function of the surfaces occurs upon adsorption of these overlayers.[48,49] The decrease is consistent with a small charge transfer from the overlayer to the substrate since this tends to reduce the magnitude of the surface dipole barrier. The Cu/Pt system is a particularly interesting system, since Cu can be underpotentially deposited on a Pt surface in an electrochemical environment.[50,51] Because of this, a SERS investigation analogous to the Ag/Pt experiment can be performed determining whether this overlayer also exhibits a partial positive charge after adsorption on Pt.

VI. SUMMARY

In this report, we have shown that only small optical fields exist at the Ag ML—Pt substrate surface indicating that this surface is an ideal testing ground for the short-range mechanism of SERS. The well-controlled growth of the Ag ML on Pt was made possible using a new thin-layer electrochemical cell. This cell allowed investigation of the pyridine—silver-monolayer interaction prior to and after activation of the Ag ML in a pyridine and Cl^- solution. We believe that the Ag^+-Pyr complex responsible for the observed SERS can only be formed during such an activation of the Ag ML. Previously, we believed that the small positive charge that exists on the underpotentially deposited Ag should promote the formation of the Ag^+-Pyr complex. However, since no SERS is observed from pyridine adsorbed on the pre-prepared Ag ML [Figs. 9 and 10(a)], this cannot be the dominant mechanism in

forming the electronically resonant complex.

From the Raman spectra, we conclude that the dominant surface complex is pyridine bound to electron-deficient Ag sites on Pt and stabilized by specifically adsorbed Cl^-. The assignment for this resonant complex is supported by photoemission and work function investigations of the Ag/Pt surface which show a small charge transfer from the metal overlayer to the underlying substrate. We found the complex was destroyed at bias potentials negative of -0.1 V, suggesting that these potentials desorbed the stabilizing Cl^- and neutralized the Ag^+-Pyr complex. The adsorbed Cl^- appeared to influence the Raman modes by shifting the ring-breathing mode at 1020 to 1023 cm^{-1}. This Cl^- influence on the adsorbed pyridine has been observed in a previous Raman study of Cl^- and pyridine adsorption on η-alumina powder sample.

We previously concluded that the chemical nature of the substrate, which is related to its electronic structure, had a secondary influence on the character of the adsorbed complex regarding its ability to support SERS through the resonant Raman process and influence the formation of the SERS active Ag^+-Pyr complex. However, one had to question why the observed SERS mode at 1020 cm^{-1} is usually absent in SERS investigations on bulk Ag substrates, except under extreme surface pretreatment. In these studies, the predominant pyridine modes are 1008 and 1037 cm^{-1} which are *not* usually associated with pyridine bound to an electron-deficient site. Although there is little doubt as to the validity of active sites such as adatoms and clusters on the bulk Ag substrate, it appears the sites may not be as electron deficient as the active sites found on Ag-coated Pt.

ACKNOWLEDGMENT

This work was supported by the U.S. Department of Energy through the office of Basic Energy Sciences under Contract No. DE-AC02-82ER12032.

[1]M. Fleischmann, P. J. Hendra, and A. J. McQuillan, Chem. Phys. Lett. **26**, 163 (1974).
[2]T. E. Furtak, in *Advances in Laser Spectroscopy*, edited by B. A. Garetz and J. R. Lombardi (Wiley, New York, 1983), p. 175.
[3]J. Gersten and A. Nitzan, J. Chem. Phys. **73**, 3023 (1980).
[4]F. J. Adrian, Chem. Phys. Lett. **78**, 45 (1981).
[5]M. Kerker, D. S. Wang, and H. Chew, Appl. Opt. **19**, 4159 (1980).
[6]D. S. Wang and M. Kerker, Phys. Rev. B **24**, 1777 (1981).
[7]S. H. Macomber and T. E. Furtak, Chem. Phys. Lett. **90**, 59 (1982).
[8]D. Roy and T. E. Furtak, J. Chem. Phys. **81**, 4168 (1984).
[9]T. E. Furtak and D. Roy, Phys. Rev. Lett. **50**, 1301 (1983).
[10]C. Pettenkofer, J. Eickmans, Ü. Ertürk, and A. Otto, Surf. Sci. **151**, 9 (1985).
[11]T. Watanabe, O. Kawanami, K. Honda, and B. Pettinger, Chem. Phys. Lett. **102**, 565 (1983).
[12]B. H. Loo and T. E. Furtak, Chem. Phys. Lett. **71**, 68 (1980).
[13]J. F. Owen, T. T. Chen, R. K. Chang, and B. L. Laube, Surf. Sci. **131**, 195 (1983).
[14]A. Regis and J. Corset, Chem. Phys. Lett. **70**, 305 (1980).
[15]T. E. Furtak, Solid State Commun. **28**, 903 (1978).
[16]J. E. Pemberton, J. Electroanal. Chem. **167**, 317 (1984).
[17]V. V. Marinyuk, R. M. Lazorenko-Manevich, and Ya. M. Koloyrkin, Solid State Commun. **43**, 721 (1982).
[18]M. P. Cline, P. W. Barber, and R. K. Chang, J. Opt. Soc. Am. B **3**, 15 (1986).
[19]T. E. Furtak and J. Miragliotta, Surf. Sci. **167**, 381 (1986).
[20]J. S. Hammond and N. Winograd, J. Electronal. Chem. **80**, 133 (1977).
[21]*Surface Polaritons*, edited by V. M. Agronovich and D. L. Mills (North-Holland, Amsterdam, 1982).
[22]S. L. McCall, P. M. Platzman, and P. A. Wolf, Phys. Rev. Lett. **79**, A381 (1980).
[23]C. A. Murray, J. Opt. Soc. Am. B **2**, 1330 (1985).
[24]Z. Kotler and A. Nitzan, J. Phys. Chem. **86**, 2011 (1982).
[25]C. F. Eagen, Appl. Opt. **20**, 3035 (1981).
[26]R. R. Bilboul, Br. J. Appl. Phys. **2**, 921 (1969).
[27]J. H. Weaver, Phys. Rev. B **11**, 1416 (1975).
[28]B. F. Schmidt and D. W. Lynch, Phys. Rev. B **3**, 4015 (1971).
[29]P. W. Barber, R. K. Chang, and H. Massoudi, Phys. Rev. B **27**, 7251 (1983).
[30]R. B. Dingle, Proc. R. Soc. London, Ser. A **201**, 545 (1950).
[31]J. A. Stratton, *Electromagnetic Theory* (McGraw-Hill, New York, 1941), Chap. 3.
[32]B. E. Conway, H. Angerstein-Kozowska, W. B. A. Sharp, and E. E. Criddle, Anal. Chem. **45**, 1331 (1973).
[33]T. Biegler, D. A. J. Rand, and R. Woods, J. Electroanal. Chem. **29**, 269 (1971).
[34]D. M. Kolb, M. Przasnyski, and H. Gerischer, J. Electronal. Chem. **54**, 25 (1974).
[35]M. T. Paffet, C. T. Campbell, and T. N. Taylor, Langmuir **1**, 741 (1985).
[36]S. H. Cadle and S. Bruckenstein, Anal. Chem. **43**, 1858 (1971).
[37]G. W. Tindall and S. Bruckenstein, Electrochem. Acta. **16**, 245 (1971).
[38]S. Stucki, J. Electroanal. Chem. **80**, 375 (1977).
[39]A. T. Hubbard, J. Electronanal. Chem. **2**, 165 (1969).
[40]S. H. Cadle and S. Bruckenstein, Anal. Chem. **44**, 1993 (1972).
[41]M. Fleishmann and I. R. Hill, in *Surface Enhanced Raman Scattering*, edited by R. K. Chang and T. E. Furtak (Plenum, New York, 1982), p. 275.
[42]T. E. Furtak and D. Roy, Surf. Sci. **158**, 126 (1985).
[43]S. C. Sun, I. Bernard, R. L. Birke, and J. R. Lombardi, J. Electroanal. Chem. **196**, 359 (1985).
[44]M. Fleischmann and I. R. Hill, J. Electroanal. Chem. **146**, 353 (1983).
[45]D. J. Rogers, S. D. Luck, D. E. Irish, D. A. Guzonas, and G. F. Atkinson, J. Electroanal. Chem. **167**, 237 (1984).
[46]D. Roy and T. E. Furtak, Chem. Phys. Lett. **124**, 299 (1986).
[47]P. J. Hendra, J. R. Horder, and E. J. Loader, J. Chem. Soc. A 1766 (1971).
[48]M. Salmeron, S. Ferrer, M. Jazzar, and G. A. Somorjai, Phys. Rev. B **28**, 6758 (1983).
[49]M. L. Shek, P. M. Stefan, I. Lindau, and W. E. Spicer, Phys. Rev. B **27**, 7277 (1983).
[50]N. Furuya and S. Motoo, J. Electroanal. Chem. **72**, 165 (1976).
[51]P. C. Andricacos and P. N. Ross, J. Electroanal. Chem. **167**, 301 (1984).